Spectroscopy of metamaterials from infrared to optical frequencies

Willie J. Padilla

Materials Science and Technology Division, Center for Integrated Nanotechnologies, Los Alamos National Laboratory, MS G756, Los Alamos, New Mexico 87545

David R. Smith

Department of Electrical and Computer Engineering, Duke University, Durham, North Carolina 27708-0291

Dimitri N. Basov

Department of Physics, University of California San Diego, La Jolla, California 92093-0319

We review both the theoretical electromagnetic response and the spectroscopic measurements of metamaterials. To critically examine published results for metamaterial structures operating in the range from terahertz to optical frequencies, we focus on protocols allowing one to extract the optical constants from experimental observables. We discuss the complexity of this task when applied to metamaterials exhibiting electric, magnetic, and magneto-optical response. The general theory of the electromagnetic response of such systems is presented and methods are described. Finally, we briefly overview possible solutions for implementing metamaterials with tunable resonant behavior. © 2006 Optical Society of America

OCIS codes: 160.3820, 300.6270, 120.2130, 160.4760.

1. INTRODUCTION

There has been unprecedented activity and excitement recently over the discovery of negative index materials (NIMs).[1] Although discovered only five years ago, research in the field has rapidly blossomed engaging a community of researchers with backgrounds in electromagnetics (EMs), optics, engineering, chemistry, physics, and materials science. Excitement in NIM stems from the ability of these materials to not only span many decades of the EM spectrum, but also to attain material response that is difficult or impossible to achieve with natural materials. The additional inherent constructed nature of these artificial materials ensures applicability for future devices.[2]

The electrodynamics of NIMs was first analyzed in 1967 by Veselago,[3] and the reversal of phenomena such as refraction, the Doppler effect, Cerenkov radiation, and radiation pressure were predicted. Discussion of negative index (NI) was also presented in the lecture notes of Mandelshtam in the early 1940s.[4] The first experimental demonstration of NI[1] was motivated by the theoretical work of Pendry *et al.* who showed that artificially constructed materials could be fabricated to exhibit an effective permittivity and permeability.[5,6]

Metamaterials constructed for NI behavior are typically formed from individual components designed to respond independently to the electric and magnetic fields of an incident EM wave. The requirements for a material to obtain NI (given by the real part of the complex refractive index $\tilde{n} = n_1 + i n_2$) are that the group $\bar{V}_g$ and phase $\bar{V}_p$ velocities be antiparallel[7]; hence the index is negative, n_1

< 0. One such way for a material to meet this requirement is through negative values of the real parts of both the electric permittivity $\epsilon_1(\omega)$ and the magnetic permeability $\mu_1(\omega)$ over a common range of frequencies. Materials that exhibit negative permittivity are not uncommon, and any metal below its plasma frequency ω_p meets this requirement. Apart from metals, composite nonconducting materials termed artificial dielectrics have been known since the 1940s, and are capable of yielding $\epsilon < 0$ over a limited frequency range.

The key to demonstration of NI was the fabrication of an artificial material that satisfied the $\mu < 0$ criterion in simultaneity with $\epsilon < 0$. Although there are natural materials capable of negative magnetic response [for example, antiferromagnets close to resonance frequencies in the far infrared reveal $\mu < 0$ (Ref. 8)], these systems are usually insulating implying a positive dielectric function in the region where the permeability is negative. The benefit of a composite material is that both response functions (ϵ, μ) can be designed to be negative, and thus one is not constrained by the limitations of mother nature.

The first experiments on NIM were performed at microwave frequencies due to the simplicity of fabrication as well as ease of complex transmission and reflection experiments.[1,9] These experiments included demonstration of one-dimensional NI, two-dimensional NI, and verification of negative refraction. Since the demonstration of NI there has been a rapid extension of the magnetic component to both higher and lower frequencies. Research groups have been pushing artificial magnetic materials to RFs for use in magnetic resonance imaging,[10] while

others have extended to terahertz (THz)[11] and mid-infrared (MIR)[12,13] frequencies. Even though the field of NI systems is still in its infancy, resonant behavior of structures designed to exhibit artificial magnetic response have already been shown to scale over 6 orders of magnitude in frequency, thus evincing their usefulness for device applications. In this paper we overview the fundamental electrodynamics of these resonant structures and discuss a series of experiments aimed at the demonstration of magnetic response at THz and higher frequencies.

2. EXPERIMENTAL TECHNIQUES AND OBSERVABLES

At frequencies above the microwave regime experimental observables suitable for the analysis of the EM response of a material include reflectance $R(\omega)$, transmission $T(\omega)$, and ellipsometric coefficients $\Psi(\omega)$ and $\Delta(\omega)$. The vast majority of natural materials do not show magnetic response ($\mu = 1$) and therefore the only relevant material parameter is complex $\tilde{\epsilon}$. The real and imaginary parts of $\tilde{\epsilon}$ can be inferred through one or several of the following procedures:

(i) a combination of $R(\omega)$ and $T(\omega)$ obtained for transparent materials can be used to extract the dielectric function through analytic expressions,

(ii) Kramers–Kronig analysis of $R(\omega)$ for opaque systems or of $T(\omega)$ for a transparent system,[14]

(iii) ellipsometric coefficients $\Psi(\omega)$ and $\Delta(\omega)$ for either transparent or opaque material can be used to determine the dielectric function through analytic expressions,

(iv) various interferometric approaches, in particular Mach–Zehnder interferometry,[15] and

(v) THz time-domain spectroscopy (TDS).[16]

Apart from protocols (i)–(iii), which are based on intensity measurements, the last two techniques are capable of yielding the optical constants directly through the analysis of the phase information. While quite a powerful technique, phase information for both the reflected and the transmitted waves is often difficult to obtain at higher frequencies. Using interferometric methods it is often possible to obtain the phase of the transmitted wave; when the sample is sufficiently well matched to free space, such that multiple reflection within the sample is minimized, then the transmitted phase is proportional to the refractive index of the sample. For matched samples, then, the index can be deduced by observation of the phase variation with either frequency or sample thickness. This technique has been explored for NI media both at microwave frequencies[17,18] and in the IR.[19]

It is worth noting that with the exception of (ii), all these protocols produce the optical constants throughout the entire frequency range where experimental data exist. The standard routines (i)–(v) have to be modified for a NIM since in this case at least four unknown functions, complex $\tilde{\epsilon}$ and complex $\tilde{\mu} \neq 1$, are jointly responsible for the behavior of experimental observables. Last we point out that if one is interested in characterizing a NI material, a refraction experiment is suitable (perhaps preferred) as this demonstrates NI directly. Indeed the issue

of NI was largely debated even after initial refraction experiments were carried out,[9] until verified by other various groups.[20]

In Fig. 1 we show a reflectance spectrum for a Lorentz oscillator modeled using the Fresnel equations shown in Eq. (2), with $\theta = 0$ and some corresponding optical constants. Reflectance (and transmission) is not a particularly intuitive material parameter. For example, the oscillator is centered at $\omega_0 = 300 \text{ cm}^{-1}$ ($33 \text{ cm}^{-1} = 1 \text{ THz}$); however, although $R(\omega)$ can be seen to start around ω_0, it asymmetrically extends to frequencies $\sim 350 \text{ cm}^{-1}$ on the high-ω end. As both $R(\omega)$ and $T(\omega)$ are absolute quantities, they are constrained to lie between 0 and 1. Thus the apparent band width is given by a combination of the natural linewidth (γ), the oscillator strength (S), and other contributions to the spectral weight at higher frequencies (ϵ_∞). Thus the form of an oscillator in $R(\omega)$ and $T(\omega)$ can be quite complex, and the situation is further complicated when two oscillators occur in the same frequency range.

The reflectance plotted in Fig. 1 is the result of a frequency-dependent dielectric contribution, as given by Eq. (2), at normal incidence. The situation is significantly more complicated if frequency-dependent $\mu(\omega)$ also exists in a material or metamaterial. In Eqs. (1) we present the Fresnel equations that determine the reflectance from a material described by the macroscopic form of Maxwells' equations at an angle θ from the surface normal, for both transverse electric (TE) and transverse magnetic (TM) polarizations. As can be seen, both $\epsilon(\omega)$ and $\mu(\omega)$ contribute to $R(\omega)$

$$R(\omega)_{\text{TE}} = \left| \frac{\cos\theta - \mu^{-1}\sqrt{\epsilon\mu - \sin^2\theta}}{\cos\theta + \mu^{-1}\sqrt{\epsilon\mu - \sin^2\theta}} \right|^2,$$

$$R(\omega)_{\text{TM}} = \left| \frac{\epsilon\cos\theta - \sqrt{\epsilon\mu - \sin^2\theta}}{\epsilon\cos\theta + \sqrt{\epsilon\mu - \sin^2\theta}} \right|^2. \qquad (1)$$
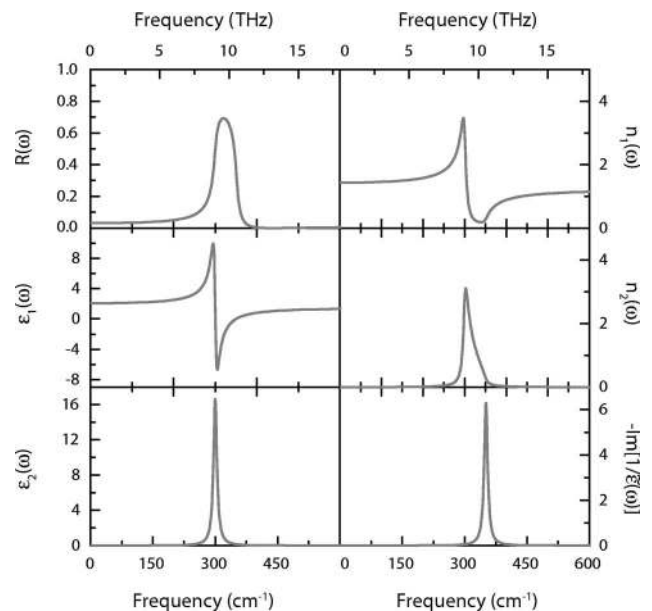

Fig. 1. Some optical constants for a Lorentz oscillator. The oscillator is modeled using Eq. (2) with the parameters given as $S = 50,000 \text{ cm}^{-1}$, $\epsilon_\infty = 1.5$, $\gamma = 10 \text{ cm}^{-1}$, $\omega_0 = 300 \text{ cm}^{-1}$.

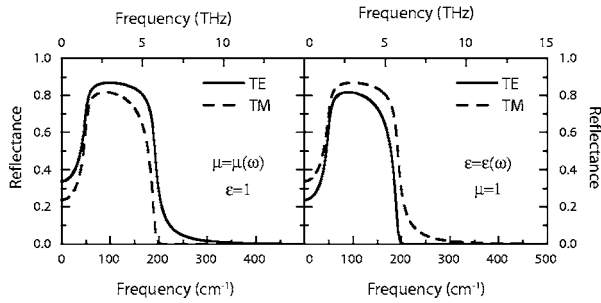Fig. 2. Oblique angle reflectance plotted for $\theta = 30°$ as determined by Eqs. (1) for both TE and TM polarizations. In the left panel the reflectance is a result of a magnetic contribution with $\epsilon = 1$ in this case. The right panel displays $R(\omega)$ for an electric oscillator $\epsilon(\omega)$ and $\mu = 1$.

At normal incidence ($\theta = 0$), the reflectance (or transmission) spectra do not allow one to discriminate between $\epsilon(\omega)$ or $\mu(\omega)$ contributions. That is, assuming magnetic and electric oscillators are of equal strength, the reflectance spectra produced by these two oscillators are identical. This is why it is important when considering metamaterials to perform measurements of both the amplitude and the phase (vector measurements). One possible way to determine whether contributions are magnetic or electric is to perform ellipsometry. In Fig. 2 we show simulated oblique angle reflectance for a magnetic oscillator (left panel) and for a electric resonator (right panel) both at $\theta = 30°$. An electric resonance is weaker for light polarization in the TE mode compared with that of the TM mode and the opposite is true for a magnetic resonance. In general, for an oblique incidence reflectance measurement, the TE/TM ratio for resonances in $\epsilon(\omega)$ is less than 1 and greater than 1 for modes associated with $\mu(\omega)$. Ellipsometry inherently measures spectra in ratios, and thus it is significantly more sensitive than other frequency-domain spectroscopies.

3. ELECTRODYNAMICS OF METAMATERIALS

A composite EM metamaterial is typically constructed from a periodic array of one or more conducting elements that determine the overall EM response of the entire structure. Straight wire or rod segments (left panel of Fig. 3) are used to achieve a negative $\epsilon(\omega)$ response, while elements termed split-ring resonators (SRRs), right panel of Fig. 3, are often used to obtain a negative $\mu(\omega)$ response. Metamaterials are microstructured or nanostructured materials designed to give an effective EM response that can be described by the macroscopic form of Maxwells' equations. They are designed and utilized to work in the effective-medium regime.[21] It is thus required that the individual elements that form these composites be much smaller than the wavelength. That is, if [a] is the characteristic length of a element from which a metamaterial is formed, and λ is the wavelength at which one would like to utilize the metamaterial, then it is necessary that ($a \ll \lambda$). This condition is relatively easy to satisfy at microwave frequencies, and values of $\lambda/a \sim 100$ have been demonstrated. However, at higher frequencies the $a \ll \lambda$ requirement is more difficult to achieve since

frequency and wavelength scale inversely. Typical values at THz frequencies of $\lambda/a \sim 10$ are achievable with conventional lithographic methods.

An array of wires or metal meshes is the simplest possible metamaterial that allows one to obtain the regime of an artificial dielectric mentioned above.[22,23] The work of Ulrich in the late 1960s and others pursued wire grid meshes and their complementary structures to form filters for the IR or THz frequencies.[24,25] Other work focused on artificial low-frequency plasmon materials,[6,26] which utilize thin straight conducting wire materials to achieve a tuned ω_p and $\epsilon(\omega)$ response. Most efforts pushing EM metamaterials to higher frequencies have been focused on the magnetic component; thus we will address this issue below, and only a brief review of the electric component will be covered.

A. Electric Metamaterials
Artificial wire composites are used at frequencies below ω_p and can be thought of as a dilute plasma. Essentially the wires, compared to a bulk metal, have a reduced number density (n), as the carriers (electrons) are restricted to the physical dimensions of the wires. The plasma frequency is given by $\omega_p^2 = 4\pi(ne^2/m^*)$, and the frequency dependence of the electric response is given by the Drude–Lorentz model as

$$\tilde{\epsilon}(\omega) = \epsilon_\infty + \frac{\omega_p^2}{\omega_0^2 - \omega^2 - i\gamma\omega}, \qquad (2)$$

where ϵ_∞ is the real part of a dielectric constant at $\omega = \infty$, ω_0 is the center frequency of the oscillator, and γ is the damping. For bulk metals the number density is typically $\sim 10^{22}$ cm^3, and thus ω_p usually occurs in the ultraviolet. In the case of infinitely long straight wire segments, $\omega_0 = 0$ and the response is given by the Drude model (a Lorentz oscillator at zero ω).[27] The plasma frequency of artificial wires in terms of the geometry of the media was worked out in Refs. 5,23 to be $\omega_p^2 = (2\pi c^2)/(a^2 \ln a/r)$, where a is the length of the unit cell, r is the radius of the wires, and c is the speed of light. Thus, for example, with dimensions such as $a = 120$ μm and $r = 44$ μm, a plasma frequency of ~ 1 THz is predicted.

In the inset to Fig. 4 we show an artificial straight wire medium fabricated for plasma frequency response in the THz regime.[28] The radius of the wires is 15 μm and the
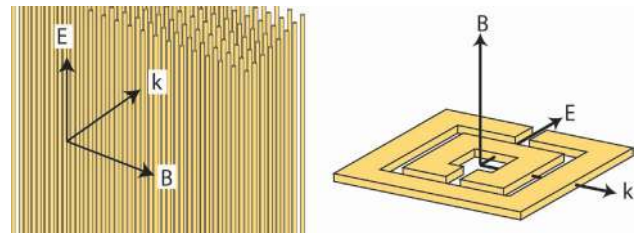

Fig. 3. Schematics of two artificial structures commonly used as EM metamaterials. Left panel shows a wire medium supporting $\epsilon < 0$ for the polarization of the incident EM wave as shown and for frequencies $\omega < \omega_p$. Right panel shows the unit cell for an artificial magnetic metamaterial. The **E** field lies along $\hat{x}$, **B** along $\hat{z}$, and **k** along $-\hat{y}$. By formation of a bipartite lattice utilizing both the electric and the magnetic metamaterial, a NI material may be constructed.
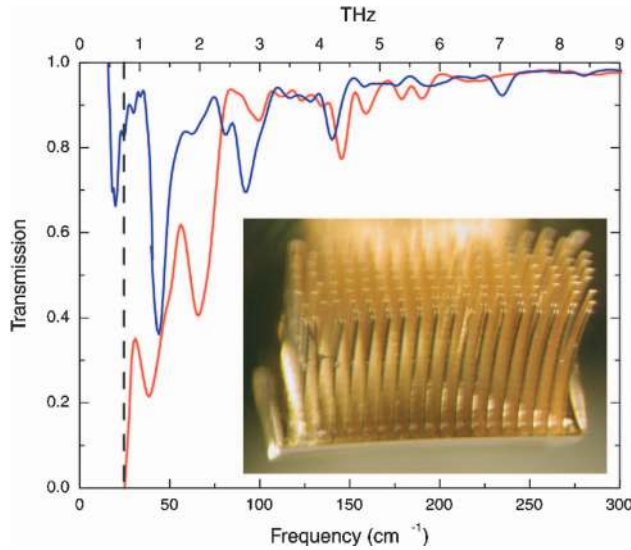
Fig. 4.   Transmission spectra for an electric metamaterial. The blue curves are for polarization perpendicular to the wires, and the red is for polarization along the wires. The transmission spectra near the predicted plasma frequency approach zero, indicating screening of the artificial medium. Inset shows a picture of the artificial wire medium.
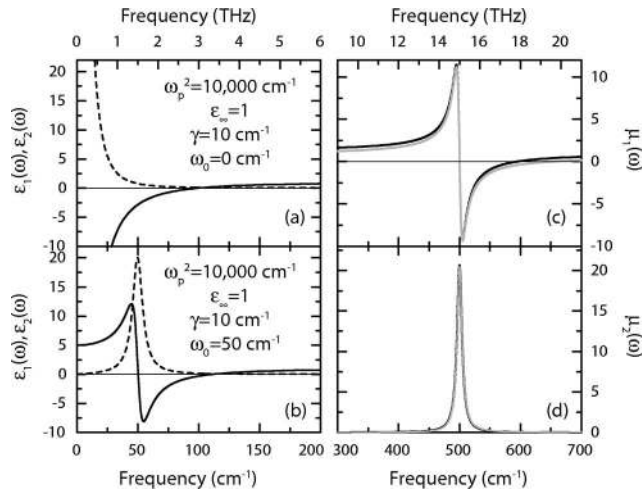

Fig. 5.   Drude–Lorentz model for an oscillator model using Eq. (2). In (a) and (b) the real part (solid curve) and the imaginary portion (dashed curve) are given. (a) A Drude oscillator ($\omega_0=0$); (b) the same oscillator but now centered at $\omega_0=50$ cm^{-1}. (c) and (d) A comparison between two magnetic oscillators given from Ref. 6 (grey curves) and a Lorentz oscillator (black curves) is shown. The real portions are plotted in (c) and the imaginary parts in (d).

lattice spacing is 120 μm, predicting $\omega_p=0.7$ THz. A polarization-dependent transmission measurement is shown in the main panel of Fig. 4. For light polarized with the electric field parallel to the wires, at frequencies above ω_p the carriers in the wires are no longer able to screen the electric field of an incident EM wave and the medium becomes transparent. However, when the polarization state of the light is rotated by 90° the medium is transparent, apart from some dips in the spectrum related to the imperfections in the wire medium. Thus the measurements are in good agreement with theory. The

electric metamaterial is reasonably in the regime of the effective-medium limit, as $\lambda/a \sim 3.6$.

In Figs. 5(a) and 5(b) we show the theoretical response of both straight wire and cut wire segments. In a continuous wire medium, the electrons can freely propagate along the length of the wire and can be described by the Drude model. In the case of cut wires the oscillator in the free case is shifted to nonzero frequencies. The cut wire model is also well described as, compared with continuous wires, now having a depolarization field, which adds capacitance to the model and thus creates a resonance. The ability to utilize both continuous wires and cut wire segments provides great versatility for tuning an artificial electric metamaterial.

B. Magnetic Metamaterials

An element, the SRR, has been the main component utilized to implement $\mu<0$ response. A single SRR is depicted in the right panel of Fig. 3. A SRR is a subwavelength resonator, meaning that its physical dimensions are much smaller than the wavelength at the resonant frequency ω_0. An incident time-varying magnetic field applied as shown in the right panel of Fig. 3 creates currents circulating around the ring. The split gap in the ring allows a capacitance to be built up and thus the resonance can be thought of as an inductive–capacitive (LC) resonance with $\omega_0 \propto \sqrt{1/LC}$. The inner counter-wound ring adds further capacitance and thus helps to meet the effective media requirement. An array of SRRs can be formed and thus a magnetic metamaterial can be described by an effective μ response.

The particular frequency-dependent form of the magnetic response for SRRs was worked out in Ref. 6 to be

$$\widetilde{\mu}(\omega) = 1 + F\frac{\omega^2}{\omega_0^2 - \omega^2 - i\gamma\omega}, \qquad (3)$$

where F is the geometric filling fraction of the unit cell, related to the dimensions of the SRRs. This form for a resonance is not causal and thus in this paper we use

$$\widetilde{\mu}(\omega) = 1 + \frac{\omega_{\mathrm{mp}}^2}{\omega_0^2 - \omega^2 - i\gamma\omega}, \qquad (4)$$

where ω_{mp}^2 is the magnetic plasma frequency. The frequency-dependent magnetic responses given by Eq. (4) and that given by Ref. 6 are quite similar [see Figs. 5(c) and 5(d) for a direct comparison].

Although the SRR is a relatively simple geometric object, it is a rather complex EM structure. This complexity stems from the fact that these materials are necessarily described by the most general form of the constitutive relations. There may be as many as 36 complex quantities to determine, and thus the standard S parameter (vector reflection and transmission measurements) yields incomplete EM information. At THz and higher frequencies where vector measurements are not common, retrieval of the optical constants is even more difficult, although methods such as ellipsometry or THz TDS may prove useful. Typically, artificial magnetic metamaterials are con-

structed from conducting elements, and thus a full EM characterization is a necessity, since an electric response is unavoidable.

SRRs have been shown to be bianisotropic,[29] and thus a brief review of the constitutive relations for such materials is in order. For a complete review, the interested reader is referred to the work of Kong.[30] The constitutive relations for bianisotropic materials may be written as[30]

$$\begin{bmatrix} \bar{D} \\ \bar{B} \end{bmatrix} = \begin{bmatrix} \bar{\bar{\epsilon}} & \bar{\bar{\xi}} \\ \bar{\bar{\zeta}} & \bar{\bar{\mu}} \end{bmatrix} \begin{bmatrix} \bar{E} \\ \bar{H} \end{bmatrix}. \tag{5}$$

In Eq. (5) the permittivities within the 2×2 matrix are tensors of rank 2. For completeness we summarize in Table 1 the various definitions for materials with different symmetry properties of the constitutive relations. The terms ξ and ζ are called the magneto-optical permittivities, and they describe coupling of the magnetic-to-electric response and electric-to-magnetic response, respectively. Then for the SRRs with the coordinate system as specified in the right panel of Fig. 3, and the expected bianisotropic nature, the material parameters are

$$\epsilon = \begin{bmatrix} \epsilon_{xx} & 0 & 0 \\ 0 & \epsilon_{yy} & 0 \\ 0 & 0 & 1 \end{bmatrix}; \quad \mu = \begin{bmatrix} 1 & 0 & 0 \\ 0 & 1 & 0 \\ 0 & 0 & \mu_{zz} \end{bmatrix}, \tag{6}$$

and the magneto-optical permittivities are

$$\xi = \begin{bmatrix} 0 & 0 & 0 \\ 0 & 0 & \xi_{yz} \\ 0 & 0 & 0 \end{bmatrix}; \quad \zeta = \begin{bmatrix} 0 & 0 & 0 \\ 0 & 0 & 0 \\ 0 & \zeta_{zy} & 0 \end{bmatrix}. \tag{7}$$

The frequency dependence of Eqs. (6) and (7) was worked out to be[29]

$$\epsilon_{xx} = a,$$

$$\epsilon_{yy}(\omega) = a + b\frac{\omega^2}{\omega_0^2 - \omega^2},$$

$$\mu_{zz}(\omega) = 1 + c\frac{\omega^2}{\omega_0^2 - \omega^2},$$

$$\xi_{yz}(\omega) = \omega_0 d\frac{\omega}{\omega_0^2 - \omega^2}, \tag{8}$$

where the coefficients a, b, c, and d are related to the geometry of the SRR and materials that are placed in the unit cell. It was further assumed that the medium was reciprocal and thus $\xi_{yz} = -\zeta_{zy}$.[31] As mentioned, since both an electric resonance and a magnetic resonance can be described with a Lorentzian oscillator, and moreover enter similarly in the Fresnel Eqs. (1) it is difficult to distinguish between the two in either a reflection or transmission experiment at normal incidence.

Equations (6) and (7) are for SRRs in one dimension; however, the form of the magneto-optical permittivities is

Table 1. Material Definitions with Respect to the Symmetries of the Constitutive Relations[a]

Material Designation	$\bar{\bar{\epsilon}}, \bar{\bar{\mu}}$	$\bar{\bar{\xi}}, \bar{\bar{\zeta}}$
Isotropic	$\propto \mathbf{I}$	$\bar{\bar{\xi}}, \bar{\bar{\zeta}} = 0$
Anisotropic	$\bar{\bar{\epsilon}}$ and/or $\bar{\bar{\mu}}$ not $\propto \mathbf{I}$	$\bar{\bar{\xi}}, \bar{\bar{\zeta}} = 0$
Biisotropic	$\propto \mathbf{I}$	$\propto \mathbf{I}$
Bianisotropic	All other cases	All other cases

[a]$\mathbf{I}$ denotes the identity matrix.

significantly more complicated in three dimensions (3D). Although the magnetic response generalizes to 3D and is isotropic, the bianisotropic SRRs add two terms to the magneto-optical permittivities, e.g., $\xi_{zy} = -\zeta_{yz}$ and $\xi_{yx} = \zeta_{xy}$, and another frequency-dependent electrical response, e.g., $\epsilon_{zz}(\omega)$, depending upon how the gap in the SRR is oriented. Thus the SRR is not an ideal magnetic material to extend to higher dimensions.

4. SPECTROSCOPY OF METAMATERIALS

The current effort to extend metamaterials to higher frequencies requires innovative approaches to characterization. Characterization methods that require the direct measurement of the transmitted and reflected phases are less convenient at submillimeter wavelengths. To circumvent this limitation, many researchers have made use solely of transmittance or reflectance measurements coupled with numerical simulations to characterize the response of high-frequency metamaterials.

The characterization of high-frequency metamaterials is further complicated by the constraints of fabrication. To date, fabrication techniques have largely been based on planar lithography, in which a single layer of a metamaterial structure is deposited on a substrate. For limited quantity proof-of-concept experiments, the processing is expensive and time-consuming, such that one plane of the sample is often all that is feasible to produce. The assignment of bulk material parameters to a single plane of a sample adds a substantial burden to the characterization effort.

In the absence of phase information, ellipsometry is a promising approach to material characterization at high frequencies. Yen *et al.* have performed a partial ellipsometric study of a planar SRR sample designed to operate at THz frequencies. This experiment illustrates both the possibilities as well as the difficulties associated with ellipsometric analysis of complex materials.[11] Three different samples of 3 μm thick copper SRRs were fabricated on a 400 μm thick quartz substrate (inset to Fig. 6) and each were characterized with both TE- and TM-polarized light. Additionally, since SRRs are known to be bianisotropic, the samples were rotated by 90 deg in the plane and were again characterized with both polarizations. The results of measurements of structures with different dimensions and geometries directly demonstrate the scalability of SRRs over a band of THz frequencies, as shown in Fig. 6.
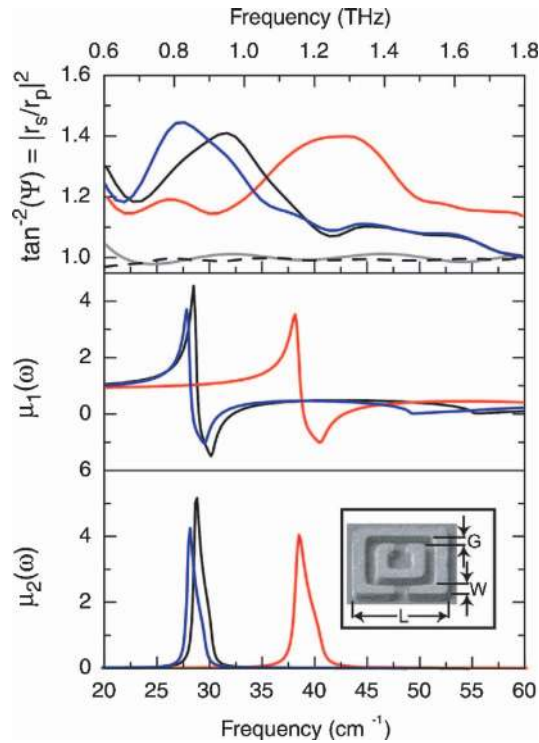
Fig. 6. Measurements of micrometer-sized SRRs designed for magnetic response at THz frequencies after Ref. 11. Inset to bottom panel shows a picture of one SRR, and the corresponding dimensions: gap between the inner and outer ring (G), the width of the metal lines (W), the length of the outer ring (L), and the lattice parameters were 2, 4, 26, and 36 μm for the sample exhibiting the highest frequency resonance (red curve); 3, 4, 32, and 44 μm (black curve), and 3, 6, 36, and 50 μm for the sample with the lowest resonant frequency (blue curve). Top panel displays the ellipsometric parameter described in the text for the three SRR samples (red, black, and blue curves). The dashed black curve and the solid gray curve are for the same measured parameter for copper and quartz, respectively. Middle and bottom panels display the real and imaginary portions of $\mu(\omega)$, respectively, as simulated for the three different SRRs.

The thin SRR planar geometry by definition is anisotropic and of finite thickness, so that the Fresnel scattering formulas become considerably more complicated than those in Eqs. (1). Moreover, because the planar sample does not possess a plane of symmetry, the magnetoelectric coupling term cannot be neglected. With at least six unknown significant material parameters (real and complex) to be determined, transmittance or reflectance measurements on the structure at several angles of incidence would be required to properly characterize the structure.

The ellipsometry ratio (the ratio of TM-to-TE polarized light), plotted in the top panel of Fig. 6, demonstrates that the SRRs have an enhanced response at the predicted THz frequencies, consistent with simulations on the identical geometries. By correlating the observed resonant frequency with that predicted from simulations, a strong case for the magnetic response of SRRs can be made. Given the complicated manner in which all the resonant terms enter into the ellipsometry formulas, a more quantitative statement about the permeability component cannot be made. However, the magneto-optical terms (ξ and ζ) manifest themselves in spectroscopy as polarization rotation or mixing, resulting in elliptically polarized light.

Signs of this cross polarization were not observable through cross-polarized measurements.

Although the bianostropic planar samples studied in Ref. 11 lead to a complication in characterization, the situation can be greatly improved by fabricating samples that possess symmetry planes in all directions. By analyzing the reflectance of symmetric structures for waves incident at nonnormal incidence, and with careful consideration of the incident polarization of the wave relative to the structure, a quantitative retrieval of the permeability should be quite feasible.

By applying ever-improving microfabrication and nanofabrication methods, researchers have made steady progress in advancing the frequency response of metamaterials upwards in frequency over the past several years. A study in 2004 (Ref. 32) reported a far-infrared resonance with aluminum SRRs 0.5 μm thick on a 0.7 μm thick silicon substrate at ~28 THz. The characterization of the SRRs was based on a transmission experiment with several laser lines $\lambda_1 = 10.86$ μm, $\lambda_2 = 9.43$ μm, and $\lambda_3 = 808$ nm. The characteristic length of the SRRs was $a = 10.48$ μm and the lattice parameter was ~15 μm. The measurements from Ref. 32 indicate that there is a difference in absorption between the SRR orientation for which a magnetic resonance is expected compared with the SRR orientation for which no resonance is expected. Although the SRR samples used in Ref. 32 are strictly outside of the effective-medium regime (since wavelengths λ_1, λ_2, and λ_3 yield a ratio of $\lambda_1/a \sim 1$), the scattering results are consistent with an enhanced resonant response in the SRR over the 20–30 THz frequency range. By reducing the size of the unit cell relative to the wavelength and symmetrizing the SRR structures, transmittance measurements combined with various sample rotations could result in a novel characterization method.

Shortly after the measurements of Chuan *et al.*[32] were presented, Linden *et al.* made use of the inherent magnetoelectric coupling in SRRs to characterize a SRR metamaterial at 100 THz.[12] In this work, transmittance and reflectance measurements were carried out at near-normal incidence for three different planar SRR samples, all having the same dimensions ($a \sim 320$ nm), but with varying lattice parameters. In these experiments the magnetic field was oriented so as to lie in the plane of the SRR arrays and the electric field was oriented along either the asymmetric direction $\hat{y}$ axis [left panel of Fig. 7(c)] or the symmetric $\hat{x}$ axis [right panel of Fig. 7(c)]. Because the incident magnetic field is perpendicular to the axes of the SRRs, the magnetic resonance of the SRR is not driven directly, and the magnetic response of the SRR must be assessed indirectly by magnetoelectric coupling as follows. When the polarization of the electric field is directed along the asymmetric $\hat{y}$ axis, a peak in $R(\omega)$ is recorded. However, when the polarization is directed along the symmetric direction, this peak disappears. The peak in $R(\omega)$ and the corresponding dip in $T(\omega)$ clearly reveal the expected SRR resonance that occurs at a wavelength near 3 μm. As a control, the authors also measure closed rings of otherwise identical dimensions and demonstrate the absence of a resonant response over the same wavelengths. The resonance of the SRR samples is consistent with simulations performed by the authors, which reveal

that rotating currents—a prerequisite for artificial magnetism—are excited within the SRRs.

The transmittance experiments of Ref. 12 provide direct evidence of enhanced SRR response at wavelengths nearing the visible. Yet, because of the complicated nature of the bianosotropic SRR sample, which possesses both resonant permittivity as well as resonant permeability and magnetoelectric coupling [see Eqs. (7)], it is difficult to extricate quantitatively the desired magnetic response. Nevertheless, the correlation of the SRR resonance with rotating currents implies that artificial magnetic structures can be designed and fabricated to operate at wavelengths much smaller than were first deemed possible. Although the expected magnetic response was shown to be considerably weaker than the electric response in these particular samples, altering the symmetry of the SRR design could result in a material whose electric and magnetoelectric responses are suppressed.

Utilizing a novel fabrication process based on LIGA, Moser *et al.* formed a metamaterial composed of planar SRRs and discontinuous wires.[33] The authors observed a resonant electromagnetic response at ~2.5 THz. Several different metamaterials were fabricated using both Ni and Au to form SRR or wire elements. The typical dimensions of the SRRs were ~80 μm. All the structures were embedded within a photoresist, transparent over the THz band, and characterized with Fourier-transform IR transmission measurements. Simulations were performed on the composite structures and compared with analytical predictions using the formulas of Pendry *et al.*[5] The experimental transmission measurements of the composite metamaterials revealed a peak in $T(\omega)$, in good agree-

Fig. 8. Magnetic metamaterial constructed from Au designed for resonance at MIR frequencies.[13] (a) Depicts how charges will flow in the device upon the application of a time-varying magnetic field directed along the $\hat{z}$ axis. (b) Shows the currents from (a) as well as the resulting image charges. The charges and image charges thus form a net circulating current resulting in a magnetic response. Upon excitation by an external electric field **E** directed along the $\hat{y}$ axis, charges will flow as shown (c), as well as image charges shown in (d), and thus a net circulation and magnetic field **B** will be created.
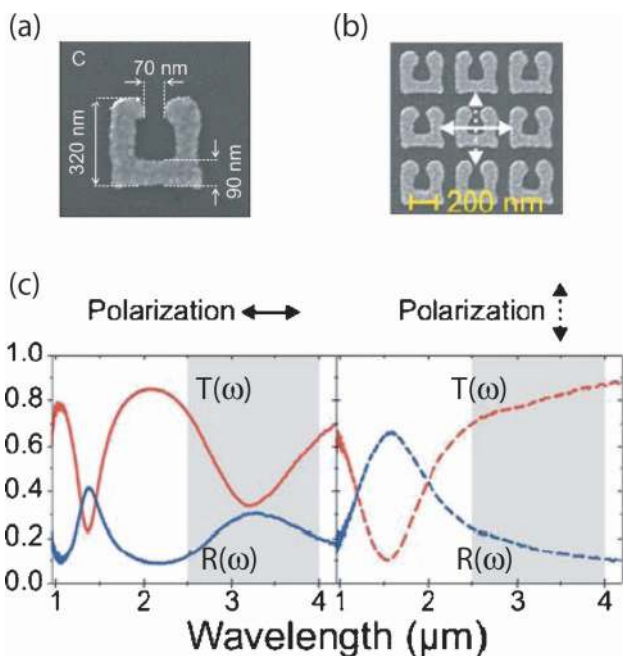

Fig. 7. SRR arrays designed to operate in MIR and near-IR frequencies (after Ref. 12). (a) A photograph of a typical SRR cell and (b) of an array used for spectroscopic studies in MIR near-IR frequencies. (c) The transmission (red) and reflectance (blue) spectra. The two polarization configurations are shown on top of the two columns. Lattice constant $a=450$ nm corresponds to nominally identical SRRs.
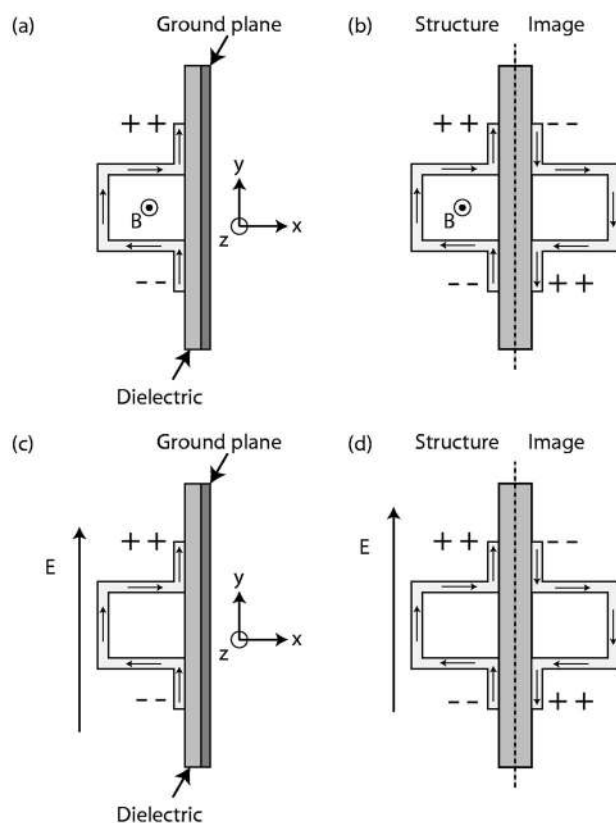
ment with that predicted by simulation and the analytic formulas. The structures were simulated with polarized light, but the experiment was carried out with unpolarized light. Characterization of the composite metamaterials was completed with the light propagating along the surface normal of the structures, and thus the magnetic field was in plane. As the experiment was performed with unpolarized light, and due to the orientation of the sample with respect to the incoming beam, contributions to $T(\omega)$ were due to both the ϵ_{yy} and ζ_{zy} terms of Eq. (5).

The examples above illustrate both the successes as well as the difficulties in scaling artificial magnetic and NIMs to high frequencies. As we have seen, one of the more complicating factors is the inherent bianisotropy of the asymmetric SRR unit cell, which places a greater burden on retrieval techniques. A way to avoid the complication of bianisotropy is to symmetrize either the individual SRRs or arrange asymmetric SRRs such that they are symmetric on average.[34] SRRs designed to minimize magnetoelectric coupling at IR frequencies have been reported, but have yet to be measured.[35] Structures that bear some similarity to those suggested in Ref. 35 have been fabricated and measured at MIR frequencies.[13] The staplelike element that forms the basis of these IR mate-

rials is depicted in Fig. 8. The staple utilizes a ground plane to complete the other half of the structure, thus achieving an effective magnetic response. These structures have a characteristic length of ~200 nm and a predicted resonant frequency of ~60 THz. The Au staples lie upon a dielectric material of 80 nm thickness above a ground plane. The structure is excited by an incident EM wave with the magnetic component lying along the $\hat{z}$ axis as shown in Fig. 8(a). The time-changing magnetic field causes circulation of charges in the structure. The ground plane allows charges (currents) to run in the image plane in the opposite direction, thus resulting in a net circulation of charges and yielding a magnetic response.

In Figs. 9(a) and 9(b) we show pictures of some of the magnetic structures of Ref. 13. Figure 9(c) shows reflection spectra for one sample (solid curve) and simulated reflectance (dotted curve). The response of one-dimensional structures was simulated using rigorous coupled-wave analysis (RCWA), and bulk properties of Au were used. The extracted frequency-dependent $\mu(\omega)$ is shown in Fig. 9(d). Good agreement between the expected resonance and the experiment is apparent.

Interestingly, although upon first inspection the staple structure would appear to be a symmetric structure and hence free of bianisotropy, because of the asymmetric drive introduced by the ground plane, the staple structure actually exhibits the same magneto-optical response as the asymmetric SRRs. In Fig. 8(c) it is shown how charges will flow under the application of an electric field. Image charges will flow in the opposite direction, and a net circulation of charges will result and a magnetic response will be exhibited. Thus just as the SRRs are bianisotropic, so is the staple structure. This turns out to be of little practical consequence in this particular experiment, however, since the driving electric field is substantially re-

duced by the presence of the ground plane. Thus, although the staple structure exhibits bianisotropy, the reduction of the driving electric field enables the magnetic properties of the SRR to be probed more or less directly. Simulations on the staple structure suggest that a frequency region in the IR should exist over which the effective permeability is negative.

The above-discussed measurements of metamaterials have involved variations of the experimental techniques (i) and (iii) discussed in Section 2. As mentioned, other techniques such as interferometric methods (iv) or THz TDS (v), while less available and convenient, may provide a more complete material characterization. These methods benefit by the addition of phase information. Recently, measurements of materials designed to exhibit NI at $\lambda \sim 2.0\ \mu$m were presented using interferometry in a near-IR range.[36] These metamaterials are different from typical metamaterials used at microwave and THz frequencies, consisting of a square array of through holes in two conducting layers separated by a dielectric all on a glass substrate [see Fig. 10(a)]. The lattice parameter is $a = 838$ nm and the diameter of the holes is $d = 360$ nm. The conducting Au layers are 30 nm thick and the dielectric is made of Al_2O_3 and is 60 nm thick. Interferometric information was obtained by forming two additional samples, one by forming wires of the metamaterial on the glass substrate and the other by adding Au wires with a particular spacing on top of the metamaterial. Then both $T(\omega)$ and $R(\omega)$ were characterized for all samples. A peak in $T(\omega)$ for the metamaterial sample occurring near 2 μm is changed to be a dip for the metamaterial wire sample. This is taken to indicate a large difference in phase between the two samples. Both $T(\omega)$ and $R(\omega)$ were simulated for the samples using RCWA, and good agreement with the experiment was obtained. Finally, extraction of
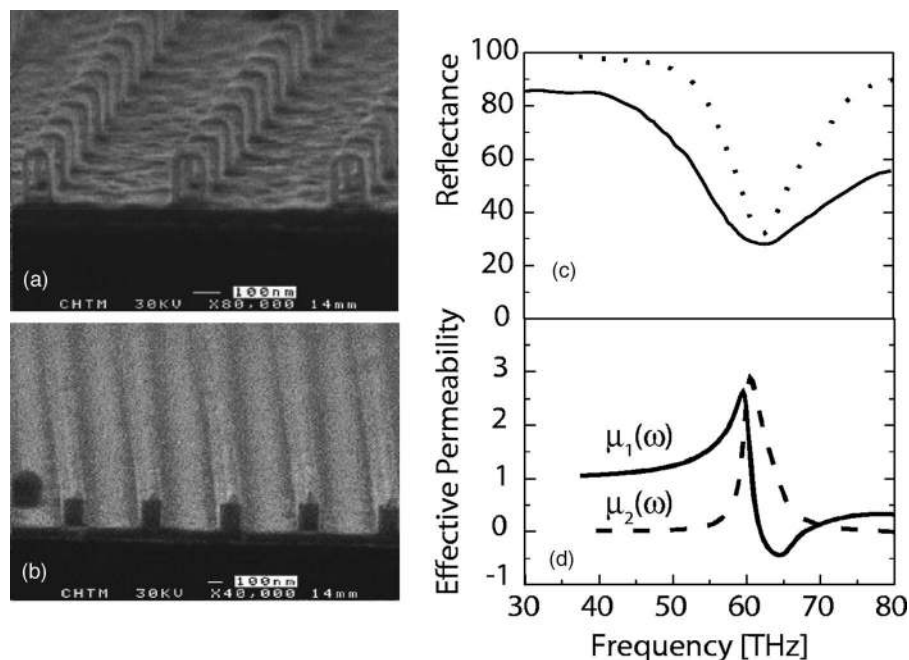

Fig. 9.   Magnetic metamaterial designed for response at MIR frequencies. Two different structures are shown in (a) and (b), all constructed from Au. In (c) reflection measurements are shown for sample c, not shown. In (d) the calculated real and imaginary parts of $\mu(\omega)$ are shown.
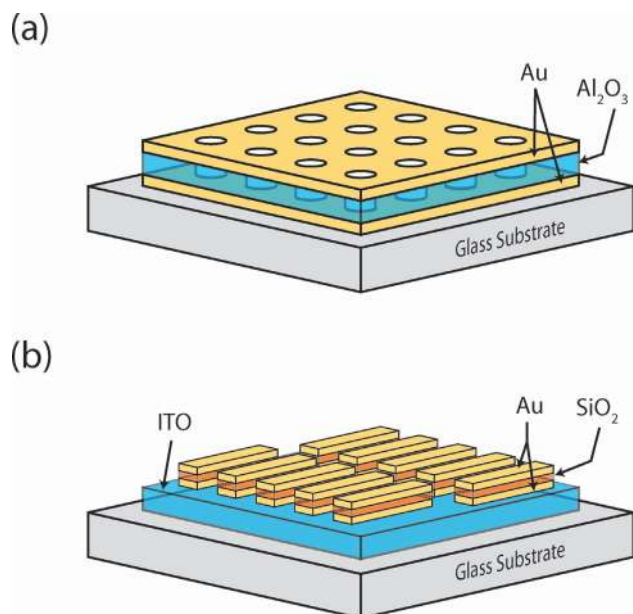
Fig. 10. Metamaterials used for response at near-IR and optical frequencies. (a) A schematic of the mulitlayer structure used in Ref. 36 consisting of an Al_2O_3 dielectric layer between two Au films with a square array of holes (pitch of 838 nm, diameter of 360 nm). (b) Shows the pairs of Au nanorods used in Ref. 19 separated by a SiO_2 layer on top of a glass substrate separated by a 180 nm layer of indium tin oxide (ITO).

the index (n) and impedance (z) was obtained from the experimental data and it was found to exhibit NI.

Another phase-dependent study focused on pairs of Au nanorods separated by a dielectric material, engineered for NI response near 1.2 μm.[19] The length and width of the nanorods was 750 and 170 nm, respectively, and had a thickness of 50 nm [see Fig. 10(b)]. A metamaterial was formed by fabricating two nanorods separated by 50 nm of a SiO_2 on 180 nm of indium tin oxide on a glass substrate. $T(\omega)$ and $R(\omega)$ were measured with a grating spectrometer using polarized light, while the phase was obtained by using polarization and walk-off interferometers. The samples were simulated using finite-difference time-domain methods, and good agreement with the experiment was obtained. Inversion of complex $T(\omega)$ and $R(\omega)$ data indicated that a NI was obtained with a maximum value of $n = -0.3$ at $\lambda \sim 1.5$ μm.

5. TUNABLE NEGATIVE INDEX AND METAMATERIALS

So far the practical implementation of NI phenomena has been successfully accomplished only in microstructured and nanostructured systems described above. The response of a given metamaterial structure is therefore rigidly determined by the geometric dimensions of the split rings and other elements. From the viewpoint of applications as well as for the purpose of the in-depth analysis of the electrodynamics of metamaterials, it is desirable to implement structures with tunable resonant properties. In this section we will briefly outline some of the possible solutions for the realization of tunable NIM systems.

We start by exploring the expression for the resonant frequency of a SRR array[6]:

$$\omega_0 = \sqrt{\frac{3}{\pi^2 \mu_0 C r^3}}, \qquad (9)$$

where r is the ring radius, μ_0 is the static magnetic permeability, and C is the capacitance per unit area between the two rings. While this analytic expression is only approximate, detailed simulations have confirmed that the resonant frequency of the SRR is indeed sensitive to this capacitance, which in turn depends on the value of the dielectric constant of the substrate ϵ_s.[37] Therefore the net result of a substrate dielectric that deviates form its freespace value is to renormalize the frequency position of the resonance by the factor $\propto 1/\sqrt{\epsilon_s}$. Therefore the easiest route to achieve tunable resonant behavior is through a modification of the dielectric constant of a substrate. SRR arrays and other types of metamaterials can be incorporated in metal-insulator-semiconductor (MIS) structures. Applying a dc electric field between the ring arrays and a semiconducting substrate allows tuning the dielectric constant of the insulating layer in a MIS device provided that the insulator is fabricated from a high dielectric constant or ferroelectric material.[38] To maintain the electric field across the insulator in the area within the splits, it is desirable to fill these structures with semiconducting polymers. Charge injection into a polymer allows one to achieve an electric field in MIS structures over large areas without appreciably changing the dc conductivity of the polymer.[38] Therefore in MIS-based devices the dielectric constant and therefore the resonant frequency can be tuned by varying the applied dc voltage. One can easily envision that each of the rings in a SRR array may be biased with a different voltage. This selective tuning of the dielectric constant may allow one to achieve the controlled distribution of the resonant frequencies over a planar array.

Alternatively, the dielectric constant of the substrate can be modified by photodoping, thus enabling a dynamical modification of metamaterial properties in accord with Eq. (9). Mode-locked lasers readily allow one to achieve high densities of photogenerated carriers in common wide-gap insulators, over subpicosecond time scales.[39] In fact, in Ref. 39 the authors succeeded in generating metallic Drude absorption that should be sufficient to dynamically shunt the gap in the SRRs. Therefore short laser pulses can be exploited for switching off the magnetic response of a SRR ring. THz TDS is ideally suited to probe the optical constants of metamaterials under photoexcitation. The structures of Ref. 13 pictured in Figs. 8 and 9 allow for the easy incorporation of dielectrics and other natural materials within the gaps of magnetic metamaterials. The added benefit of the ground permits dc bias of materials between the gaps.

6. SUMMARY AND OUTLOOK

We have detailed the expected spectroscopic response from metamaterials consisting of both electric and magnetic artificial materials. The frequency-dependent form for each of these structures has been analyzed and the difficulty of retrieval of the optical constants from experimental observables has been stressed. It is suggested that

future characterization of metamaterials at THz and higher frequencies take advantage of vector measurements (phase and amplitude), such as ellipsometry, THz TDS, or Mach–Zehnder interferometry. The artificial magnetic metamaterial in particular is a difficult structure to thoroughly characterize. This is due to the fact that, although it is designed to give a magnetic resonant response at a frequency ω_0, it exhibits an undesirable electric resonance at the same frequency, thus complicating its use and characterization. A simpler alternative route is use of more symmetric structures that do not exhibit a bianisotropic response.

The extension of metamaterials to the dynamical regime has been reviewed. Several possible methods have been suggested, all of which are particularly suited for THz frequencies, a region of the EM spectrum lacking significant natural material response.

ACKNOWLEDGMENTS

REFERENCES AND NOTES

1. D. R. Smith, W. J. Padilla, D. C. Vier, S. C. Nemat-Nasser, and S. Schultz, "Composite medium with simultaneously negative permeability and permittivity," Phys. Rev. Lett. **84**, 4184–4187 (2000).
2. J. B. Pendry and D. R. Smith, "Reversing light with negative refraction," Phys. Today **57**, 37–45 (2004).
3. V. G. Veselago, "The electrodynamics of substances with simultaneously negative values of ϵ and μ," Sov. Phys. Usp. **10**, 509–514 (1968).
4. L. I. Mandelshtam, "Lectures on some problems of the theory of oscillations (1944)," in *Complete Collection of Works* (Academy of Sciences, 1950), Vol. 5, pp. 428–467 (in Russian).
5. J. B. Pendry, A. J. Holden, W. J. Stewart, and I. Youngs, "Extremely low frequency plasmons in metallic mesostructures," Phys. Rev. Lett. **76**, 4773–4776 (1996).
6. J. B. Pendry, A. J. Holden, D. J. Robbins, and W. J. Stewart, "Magnetism from conductors and enhanced nonlinear phenomena," IEEE Trans. Microwave Theory Tech. **47**, 2075–2084 (1999).
7. This is a valid requirement for isotropic materials; however, the situation is more complicated for anisotropic and bianisotropic materials, and perhaps the requirement $\bar{V}_g \cdot \bar{V}_p < 0$ should be conisdered.
8. A. J. Sievers III and M. Tinkham, "Far-infrared exchange resonance in ytterbium iron garnet," Phys. Rev. **124**, 321–325 (1963).
9. R. A. Shelby, D. R. Smith, and S. Schultz, "Experimental verification of a negative index of refraction," Science **292**, 77–79 (2001).
10. M. C. K. Wiltshire, J. B. Pendry, I. R. Young, D. J. Larkman, D. J. Gilderdale, and J. V. Hajnal, "Microstructured magnetic materials for RF flux guides in magnetic resonance imaging," Science **291**, 849–851 (2001).
11. T. J. Yen, W. J. Padilla, N. Fang, D. C. Vier, D. R. Smith, J.

B. Pendry, D. N. Basov, and X. Zhang, "Terahertz magnetic response from artificial materials," Science **303**, 1494–1496 (2004).
12. S. Linden, C. Enkrich, M. Wegener, J. Zhou, T. Koschny, and C. M. Soukoulis, "Magnetic response of metamaterials at 100 terahertz," Science **306**, 1351–1353 (2004).
13. S. Zhang, W. Fan, B. K. Minhas, A. Frauenglass, K. J. Malloy, and S. R. J. Brueck, "Midinfrared resonant magnetic nanostructures exhibiting a negative permeability," Phys. Rev. Lett. **94**, 37402 (2005).
14. F. Wooten, *Optical Properties of Solids* (Academic, 1972).
15. For example, see M. Born and E. Wolf, *Principles of Optics* 6th ed. (Cambridge U. Press, 1997), p. 312.
16. D. Grischkowsky, S. Keiding, M. van Exter, and Ch. Fattinger, "Far-infrared time-domain spectroscopy with terahertz beams of dielectrics and semiconductors," J. Opt. Soc. Am. B **7**, 2006–2015 (1990).
17. D. R. Smith, Department of Electrical and Computer Engineering, Duke University, Durham, N.C. 27708 (personal communication, 2005).
18. K. Aydina, K. Guven, C. M. Soukoulis, and E. Ozbay, "Observation of negative refraction and negative phase velocity in left-handed metamaterials," Appl. Phys. Lett. **86**, 124102 (2005).
19. V. M. Shalaev, W. Cai, U. Chettiar, H.-K. Yuan, A. K. Sarychev, V. P. Drachev, and A. V. Kildishev, "Negative index of refraction in optical metamaterials," http://xxx.lanl.gov/abs/physics/0504091.
20. C. G. Parazzoli, R. B. Greegor, K. Li, B. E. C. Koltenbah, and M. Tanielian, "Experimental verification and simulation of negative index of refraction using Snell's law," Phys. Rev. Lett. **90**, 107401 (2003).
21. T. Koschny, M. Kafesaki, E. N. Economou, and C. M. Soukoulis, "Effective medium theory of left-handed materials," Phys. Rev. Lett. **93**, 107402 (2004).
22. R. N. Bracewell, "Analogues of an ionized medium," Wireless Eng. 31, 320–326 (1954).
23. W. Rotman, "Plasma simulation by artificial dielectrics and parallel-plate media," IRE Trans. Antennas Propag. **AP10**, 82–95 (1962).
24. R. Ulrich, "Far-infrared properties of metallic mesh and its complementary structure," Infrared Phys. **7**, 37–55 (1966).
25. T. Timusk and P. L. Richards, "Near millimeter wave bandpass filters," Appl. Opt. **20**, 1355–1360 (1981).
26. J. B. Pendry, A. J. Holden, D. J. Robbins, and W. J. Stewart, "Low frequency plasmons in thin-wire structures," J. Phys.: Condens. Matter **10**, 4785–4809 (1998).
27. If the self-inductance of the wires is sufficiently large, by design, then the effective mass of the electrons may be renormalized, and a factor in addition to the number density must be taken into account. See Ref. 5.
28. D. Wu, N. Fang, C. Sun, X. Zhang, W. J. Padilla, D. N. Basov, D. R. Smith, and S. Schultz, "Terahertz plasmonic high pass filter," Appl. Phys. Lett. **83**, 201–203 (2003).
29. R. Marques, F. Medina, and R. Rafii-El-Idrissi, "Role of bianisotropy in negative permeability and left-handed metamaterials," Phys. Rev. B **65**, 144440 (2002).
30. J. A. Kong, *Electromagnetic Wave Theory* (Wiley, 1990).
31. Media are reciprocal if $\bar{\bar{\epsilon}} = \bar{\bar{\epsilon}}^T$ and $\bar{\bar{\mu}} = \bar{\bar{\mu}}^T$ and $\bar{\bar{\xi}} = -\bar{\bar{\zeta}}^T$, where T denotes the transpose. For example, see Ref. 30.
32. A.-C. Hsu, Y.-K. Cheng, K.-H. Chen, J.-L. Chern, S.-C. Wu, C.-F. Chen, H. Chang, Y.-H. Lien, and J.-T. Shy, "Far-infrared resonance in split ring resonators," Jpn. J. Appl. Phys., Part 1 **43**, L176–L179 (2004).
33. H. O. Moser, B. D. F. Casse, O. Wilhelmi, and B. T. Saw, "Terahertz response of a microfabricated rod-split-ring-resonator electromagnetic metamaterial," Phys. Rev. Lett. **94**, 63901 (2005).
34. W. J. Padilla, "Group theoretical description of artificial magnetic metamaterials utilized for negative index of refraction," http://xxx.lanl.gov/abs/cond-mat/0508307.
35. S. O'Brien and J. B. Pendry, "Magnetic activity at infrared frequencies in structured metallic photonic crystals," J. Phys.: Condens. Matter **14**, 6383–6394 (2002).
36. S. Zhang, W. Fan, N. C. Panoiu, K. J. Malloy, R. M.

Osgood,and S. R. J. Brueck, "Experimental demonstration of near-infrared negative-index metamaterials," Phys. Rev. Lett. **95**, 137404 (2005).

37. T. Weiland, R. Schuhmann, A. M. Vetter, D. R. Smith, D. C. Vier, and S. Schultz, "*Ab initio* numerical simulation of left-handed metamaterials: comparison of calculations and experiments," J. Appl. Phys. **90**, 5419–5424 (2001).

38. Z. Q. Li, G. M. Wang, K. J. Mikolaitis, D. Moses, A. J. Heeger, and D. N. Basov, "An infrared probe of tunable dielectrics in metal-oxide-semiconductor structures," Appl. Phys. Lett. **86**, 223506 (2005).

39. J. Shan, F. Wang, E. Knoesel, M. Bonn, and T. F. Heinz, "Measurement of the frequency-dependent conductivity in sapphire," Phys. Rev. Lett. **90**, 247401 (2003).